Catalysis Today 156 (2010) 124–131

Contents lists available at ScienceDirect

Catalysis Today

journal homepage: www.elsevier.com/locate/cattod

Partial oxidation of propane to acrolein in a dual bed inert membrane reactor

C. O'Neill[1], E.E. Wolf*

Chemical Engineering Department, University of Notre Dame, Notre Dame, IN 46556, United States

ARTICLE INFO

Article history:
Available online 24 March 2010

Keywords:
Membrane
Catalytic partial oxidation
Propane
Propylene
Acrolein

ABSTRACT

The partial oxidation of propane to acrolein is studied in a dual bed membrane reactor. A porous membrane tube is used to feed oxygen to the annular catalyst beds surrounding the porous section of the membrane tube. The distributed oxygen feed in the membrane tube lowers the partial pressure of oxygen in each bed increasing selectivity to the partially oxidized product over total oxidation. The first bed contained a V/MgO catalyst for the partial oxidation of propane to propene. The second bed consisted of a BiMo catalyst to convert propene to acrolein. Studied were conducted first in each bed separately to determine operating conditions in each bed and then in a dual bed configuration.

The separate inert membrane reactors show improvement in selectivity of few % in comparison to fixed bed reactors. On the other hand when using both membrane reactors combined in a dual bed configuration a major improvement in acrolein selectivity of up to 21% was obtained. Catalysts characterization by surface area, X-ray diffraction, and X-ray photoelectron spectroscopy showed that the improvement was due to the distribution of the oxygen flow rate through the membrane in the second membrane reactor which prevented the deactivation of the BiMo catalyst.

1. Introduction

Prior modeling studies in our group [1] have demonstrated improvements in the selectivity of the partial oxidation products in the inert membrane reactor (IMR) system over a fixed bed reactor (FBR) in both the propane oxidative dehydrogenation (ODH) to propylene and propylene oxidation to acrolein (POA) reactions. Kinetics studies of these reactions show that due differences in the oxygen dependence in the reaction rates complete oxidation reactions are favored over the selective oxidation reactions [2–14]. Selective oxidation reactions for propane and propylene are about zero order in oxygen while the complete oxidation reactions are first order with respect to oxygen. This difference in the kinetics lend support to the use of membrane reactors for the selective oxidation of both propane and propylene, as a membrane tube can be utilized to distribute oxygen along the length of the catalyst bed and therefore reduce the local partial pressure of oxygen in the reaction zone.

The production of acrolein, a valuable oxygenated product, is currently derived from propylene. The utilization of propane in the production of oxygenated C_3 hydrocarbons and acrolein provides an economic incentive due to the lower cost of alkanes. The direct conversion of propane to acrolein has been studied in literature in an attempt to develop a one-step process [15–20] but such efforts have had little success with a maximum yield of 8% reported in the open literature [18]. The title reaction has also been studied in a catalytic membrane reactor in which the catalyst was part of the membrane wall [15].

The direct conversion of propane requires the dehydrogenation of C_3 to propylene (C_3=) and the oxidation of the olefin to acrolein. The necessity for using different reaction conditions for each reaction makes it more advantageous to utilize two separate reactors instead of a one-step process. Interesting results obtained by Sinev et al. [19] showed that acrolein yields could be increased by combining an ODH and POA catalysts in two beds in a single reactor. From such results it was proposed that an intermediate is formed over the ODH catalyst that produces a yield to acrolein superior than that propylene over the POA catalyst. The benefit seen from consecutive reaction beds, coupled with the difficulty in developing a catalyst for a one-step process, makes improvements to the two-bed process a more viable alternative.

The results presented in this paper were obtained by combining the consecutive reaction network of the partial oxidation of propane to acrolein with the use of a membrane reactor. A dual bed membrane reactor was used to carry out the oxidative dehydrogenation of propane to propylene in the first bed followed by the partial oxidation of propylene to acrolein in the second bed. The dual bed membrane reactor provides the opportunity for a more selective and cost effective process for the production of acrolein.

* Corresponding author. Tel.: +1 574 6315897.
E-mail address: ewolf@nd.edu (E.E. Wolf).
[1] Current address; Air Products, United States.

0920-5861/$ – see front matter © 2010 Elsevier B.V. All rights reserved.
doi:10.1016/j.cattod.2010.02.041

2. Experimental

2.1. Catalyst preparation

The catalysts used in the selective oxidation reactions of propane and propylene are V/MgO and BiMo oxide, respectively, prepared following methods reported in the literature without further optimization.

The V_2O_5 supported on MgO catalyst (V/MgO) was prepared by wet impregnation of vanadium oxide onto a MgO support [6]. 5.3 mL of ammonium hydroxide was added to 243.3 mL of reagent water resulting in a 2 wt% of ammonia solution. 1.24 g of ammonium metavanadate (NH_4VO_3) was added to the ammonia solution under constant stirring. The solution is heated up to 70 °C at which point 3.0 g of MgO are added to the solution which is further evaporated for 4 h and dried overnight at room temperature yielding a white powder. The dried powder is calcined at 550 °C for 6 h resulting in a yellow colored catalyst. After calcination, the catalyst was first pelletized and the resulting pellets were broken up and sieved to select particles between 600 μm and 1 mm for use in catalytic activity studies.

The BiMo oxide catalyst was prepared according to one the methods described in the literature [21]. Bismuth nitrate and ammonium heptamolybdate precursors solutions were prepared separately. Solution A contained 24.2 g of $Bi(NO_3)_3{\cdot}5H_2O$, 91 mL of water and 9 mL of nitric acid, and solution B consisted of 100 mL of water containing 8.8 g of $NH_4Mo_7O_{24}{\cdot}4H_2O$. Solution A was added dropwise to solution B at 1 mL/min under constant stirring maintaining the pH at 7 by addition of NH_4OH. The resulting co-precipitate formed a yellow solution, which after evaporation overnight at 90 °C, yielded a solid that was further dried for 2 days at room temperature. The dried solid was further calcined at 450 °C for 8 h yielding a yellow pale material. The catalyst was first pelletized and the resulting pellets were broken up and sieved to select particles between 600 μm and 1 mm for use in catalytic activity measurements. Each of these catalysts was characterized in a calcined (pre-reaction) and reduced (post-reaction) state.

2.2. Catalyst characterization

Total BET surface area measurements were carried out on a Monosorb (Quantachrome) instrument. Catalyst samples (50–100 mg of catalyst) were outgassed at 200 °C to remove any adsorbed water from the surface. Following outgassing, the sample was exposed to a gas stream containing 30% nitrogen in He and a liquid nitrogen bath was used to immerse the sample holder into it.

X-ray diffraction analysis was performed in a powder diffractometer using Cu Kα radiation (Scintag Inc.). The catalyst powders were sieved to particles less than 600 μm and XRD measurements were conducted in air after calcination before reaction and after reactor use.

X-ray photoelectron spectroscopy (XPS) measurements for the V/MgO and BiMo catalysts were conducted in a Kratos XSAM-800 spectrometer equipped with an Al Kα source (energy = 1.489 keV). The electron energy transitions analyzed were Mg 2p, V_2O_5 $2p_{3/2}$ and Bi $4f_{7/2}$. No statistically significant shifts of binding energies (BE) were observed due to charging effects when results were obtained using MgO, V_2O_5 and BiMo standards or obtained using and electron flood gun. Binding energies are referred to C-1s levels (285.0 eV). Surface composition was calculated from the ratio of the integrated intensity of the peak corrected by the corresponding sensitivity factor [24], with a precision estimated at about 10%. Powder samples were sieved to less than 600 μm and mounted on a XPS sample holder using a carbon tape. XPS analysis of the catalyst samples was conducted before reaction and ex situ calcination (pre-reaction) and after reaction.

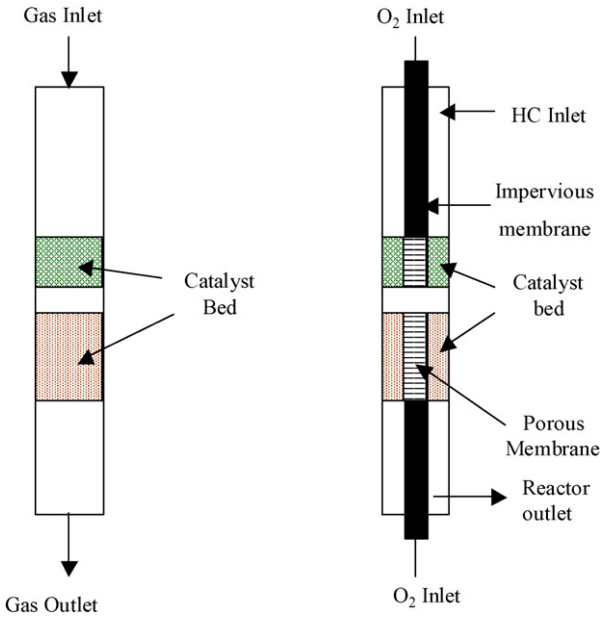

Fig. 1. (a) FBR and (b) IMR schematics in a dual bed configuration.

Fourier transform infrared spectroscopy (FTIR) experiments were conducted in a 6020 Galaxy Series FT-IR (Mattson Instruments) spectrometer. An in situ IR cell equipped with Cesium Iodide IR windows was used to conduct experiments in transmission mode on wafers prepared by pressing to 8000 psi catalyst powders that were sieved to less than 90 μm. The IR cell has a catalyst holder that was heated by cartridge heaters and the temperature was maintained constant by a PID temperature controller. The flow rates were controlled by the feed flow system described below.

2.3. Catalytic reactors

Activity and selectivity measurements were conducted in a standard tubular fixed bed reactor (FBR) and a distributive inert membrane reactor (IMR). The FBR (Fig. 1a) consisted of a quartz tube of 9.3 mm and 12.5 mm ID and OD, respectively and 12.5 cm long with the bed located in the middle of the reactor. Catalyst beds are supported by quartz wool and the feed gasses flow down through the catalyst beds into an on-line gas chromatograph (GC) sampling valve. A thermocouple inserted in a quartz thermowell is positioned concentrically inside the reactor tube within the catalyst bed. The reactor is heated with a heavy insulated flexible heating tape and the catalysts temperature is maintained constant by a programmable temperature controller. All gas flows were fed into the reaction system by computer controlled electronic mass flow controllers (MFC). Special software was used to control the MFC and specify the flow rates and run time of the reactants.

A schematic of the dual bed inert membrane reactor is shown in Fig. 1b. It consists of two concentric tubes of 18.7 mm and 21.8 in. ID and OD, respectively, leaving an annular space in between where the catalysts beds are positioned. The outer tube is made of quartz whereas the inner tube is the membrane part of the reactor.

The membrane tube consists of two separate alumina tubes of 9.37 mm ID. The first tube is a non-porous segment 12 cm long and the second is 25 mm long segment of porous alumina (US Filter). The porous segment is capped at one end with a mixture of crushed alumina and ceramic glaze dried at room temperature and baked at 990 °C. The non-porous and porous alumina tubes are bonded with ceramic glue (Respond 989 – Cotronics) at 200 °C. After the

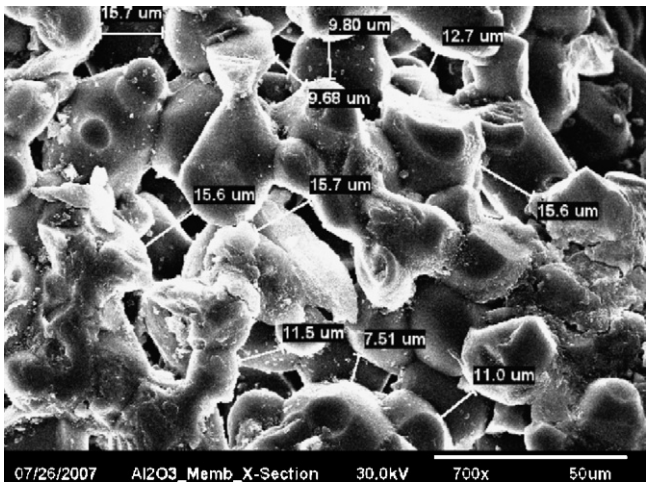

Fig. 2. SEM image of the porous alumina membrane tube at magnification 700. The average pore diameter is 12.3 μm.

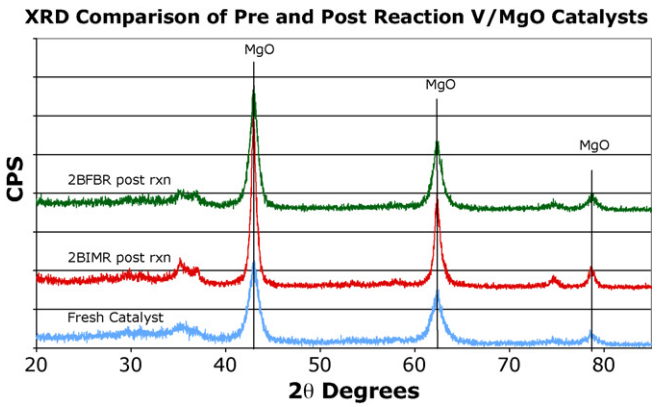

Fig. 3. X-ray diffraction patterns of the V/MgO catalyst under calcined (bottom), post-reaction 2B-IMR (middle), and post-reaction 2B-FBR (top).

desired reaction length of the porous segment is determined by the amount of catalyst to be used, a glaze coating is applied to seal off the remaining undesired porous area. The membrane tube thus prepared is baked for 12 h at 900 °C. This procedure was developed to save on the use of expensive porous alumina tubes.

An SEM image of the porous alumina membrane (Fig. 2) shows the highly porous structure and the large pore diameters of the membrane. The average pore size of the alumina is 12.3 ± 2.2 μm. The dimensions of select pores are shown to demonstrate the general order of magnitude and the variation among the pore diameters.

Each membrane tube is capped at one end so that only the fraction in contact with the catalysts bed is porous. This design was adopted to prevent mixing the gases flowing in the inner tube (oxygen) and in the annular space (propane) which would have negated the potential advantages of the membrane reactor configuration. Membrane tubes were used in an inverted configuration in the dual bed reactor to provide independent oxygen feed to each catalyst bed.

Propane and helium were fed into the outer annular space of the reactor flowing down through the catalyst beds. Oxygen was fed into the inner concentric tube flowing into the annular space through the porous segment of the membrane alumina tube. The reactor is heated for approximately 5 cm to preheat the feed and maintain the catalyst bed temperature. The catalyst beds are supported by quartz wool positioned on top of a porous quartz frit, which is open at the center to allow the membrane tube to pass through. Temperature in each bed was measured by thermocouples inserted directly into the catalyst bed from side ports on the quartz reactor tube. The reactor was heated with heavy insulated flexible heating tape and the temperature was regulated by a programmable temperature controller using the thermocouples signal as feedback. In the dual bed reactor configuration additional quartz wool was packed between the two catalyst beds, and a second heating tape and thermocouple were used and controlled by a second programmable temperature controller to maintain the temperature of the second bed constant.

Reactor effluents flow through heating tapes to prevent condensation of water and the heavier hydrocarbons products into a 6-port sampling valve for GC analysis. An HP 5890 GC, equipped with both a thermal conductivity detector (TCD) and a flame ionization detector (FID was used for analysis of the effluent gases. Two columns in series-parallel configuration were used. The sample is injected first into a 6 ft × 1/8 in. Hayesep Q 80/100 column (Alltech) connected to an air actuated 6-port switching valve and then to a second 15 ft × 1/8 in. 60/80 Carboxen-1000 (Supelco) column. The switching valve is automatically actuated to direct the He carrier gas flow with the sample to the FID for hydrocarbon analysis or to continue to the second column followed into the TCD for light gas analysis. The GC is run in a temperature controlled mode beginning with at 80 °C for 25 min and then ramping up at a rate of 25 °C/min up to 160 °C.

The carbon balance for most runs was within 5% error but it was higher when oxygen deficient feeds were used. For simplicity, the selectivity of only the main products, propylene, acrolein, CO and CO_2 are listed. The other products not listed are small amount of methane, and ethane and ethylene from C_3 cracking and partially oxygenated C_3 such as propanol, acetone and acrylic acid, all present in concentrations in the 1–3% range.

3. Results and discussion

3.1. Surface area

The specific surface areas of V/MgO and bulk Bi–Mo oxide catalyst samples, were significantly different. The MgO support has a BET surface area of 71.2 m^2/g and addition of vanadium oxide species reduced the surface area of V/MgO to 56.0 m^2/g. The bulk BiMo catalyst has a surface area of only 3.5 m^2/g, typical of bulk oxides. Despite the low surface area, the BiMo catalysts maintained a reasonable yield of about 20% for the POA reaction.

3.2. X-ray diffraction

Diffraction patterns of V/MgO catalysts obtained in air after calcination and post-reaction conditions are shown in Fig. 3. The calcined V/MgO catalyst shows three broad lines for MgO at 2θ of 43.0°, 62.3°, and 78.5° corresponding to the three main diffraction lines of the MgO. There is an absence of lines for V_2O_5 in the diffraction pattern, as they should appear between 20° and 35° possible due to having an amorphous nature or because they form a thin film monolayer that does not yield diffraction lines. No detectable change in structure seems to occur after reactor use in either reactor system.

Fig. 4 shows the pre- and post-reaction diffraction patterns for the BiMo oxide catalyst. The crystalline structures of BiMo oxides are evident in all three patterns shown and are representative of the α-($Bi_2Mo_3O_{12}$) and γ-(Bi_2MoO_6) phases of BiMo confirming that the BiMo oxide catalyst is a mixture of at least two of the three BiMo oxide phases.

The XRD patterns of the fresh and post-reaction IMR catalysts shows little change for peaks corresponding to both the α- and

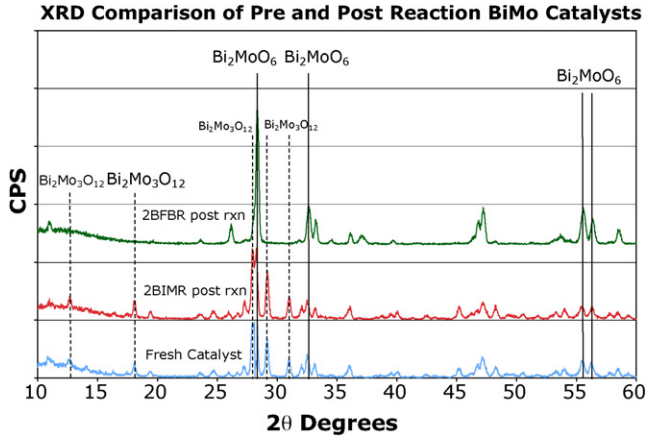

Fig. 4. XRD patterns for the BiMo oxide catalyst: (bottom) calcined, (middle) post-reaction 2B-IMR and (top) post-reaction 2B-FBR, (—) Bi_2MoO_6 and (- - -) $Bi_2Mo_3O_{12}$.

Table 1
XPS results for the V/MgO catalyst.

Conditions	V/MgO catalyst			
	BE (eV)	V_2O_{5s} (%)	BE (eV)	MgO_s (%)
Calcined	49.5	28.9	517.3	71.0
Post-reaction 2B-IMR	49.5	21.0	517.3	78.9
Post-reaction 2B-FBR	49.5	22.9	517.3	77.1

γ-phases of BiMo oxide. Obvious differences can be seen in the post-reaction 2B-FBR catalyst diffraction pattern, which shows peaks only for the γ-phase of BiMo oxide, as the low angle peaks corresponding to the α-phase are not present. This lack of α-phase peaks demonstrates a change in the crystal structure of the BiMo oxide catalyst upon reaction in the 2B-FBR, not seen after reaction in the 2B-IMR.

The different phases present among the pre- and post-reaction XRD patterns of the BiMo oxide catalysts are significant for the POA reaction as the three BiMo oxide phases have varying activity and selectivity for the POA reaction. γ-Phase BiMo oxide is the least active and selective of the three phases [10,21–23], and the main bulk phase detected in the post-reaction 2B-FBR catalyst. The absence of the more selective α- and β-phase BiMo oxides is the cause for the reduction in selectivity to acrolein observed in the 2B-FBR as opposed to the 2B-IMR where the α-phase is still present.

4. X-ray photoelectron spectroscopy

Surface analyses of the catalysts were conducted pre- and post-reaction conditions by ex situ XPS. As with the ex situ XRD experiments, XPS experiments identify changes to the catalyst after exposure to different conditions (including air during transfer to the XPS equipment) and under the UHV conditions of the XPS apparatus. Thus, the XPS results can be extrapolated to reaction conditions only if the surface is not affected due to exposure to air and vacuum, which seems to be the case in the results obtained. Tables 1 and 2 summarize the XPS results for the V/MgO and BiMo oxide catalysts, respectively, in terms of binding energies (BE) and surface ratios.

Table 2
XPS results for the BiMo oxide catalyst.

Conditions	Bio-oxide catalyst				
	BiMo oxide (eV)	%	Bi_2MoO_6 (eV)	%	Ratio
Calcined	160.0	42.3	158.3	25.3	1.7
Post-reaction 2B-IMR	160.0	32.3	158.3	22.2	1.4
Post-reaction 2B-FBR	160.0	0.00	158.3	62.5	0

The BE of the Mg 2p and V $2p_{3/2}$ transitions are unchanged at 49.5 eV and 517.3 eV, respectively for any of the conditions analyzed. These BE correspond to transitions from V^{5+} and Mg^{2+} oxidation state, respectively [24]. The difference among these samples is in the fraction of V_2O_5 on the catalyst surface. The fresh catalyst has about 29% vanadium on the surface in the form of V_2O_5 which is reduced to about 22% after reaction. The decrease in the amount of surface V_2O_5 is possibly due to the mechanism for the ODH reaction which can occur via reaction with surface oxygen and gas phase propane to form propylene [25–27]. The reduction of the surface through this reaction removes some of the oxygen in the V_2O_5 decreasing the overall percentage of V_2O_5 on the catalyst after reaction, as seen in the XPS results. The post-reaction catalysts show similar surface concentrations of V_2O_5, for the FBR and IMR configurations indicating that the V_2O_5 has a similar structure and composition in either reactor environment.

The BiMo oxide catalysts were also examined by XPS in both fresh and post-reaction conditions with the results tabulated in Table 2. Bi peaks in the XPS from the $4f_{7/2}$ transition indicate the presence of two main surface species that can be identified as Bi_2MoO_6 (γ) at a BE of 158.3 eV and other BiMo oxides at a BE of 160.0 eV [24]. The calcined BiMo oxide catalyst shows peaks for both the γ-phase and other BiMo oxide phases, consistent with the XRD patterns in Fig. 3. The main differences amongst the pre- and post-reaction catalysts are in the ratio of the α-/γ-phases on the surface of the BiMo oxide catalyst which decreases from 1.67 to 1.45 to 0 for the fresh, post-reaction IMR, and post-reaction FBR, respectively. This demonstrates that the calcined and post-reaction IMR BiMo oxide catalysts contain a mixture of the BiMo oxide phases while the post-reaction FBR catalyst has only the γ-phase in agreement with the XRD results. The XPS results demonstrate a clear difference in the phases present for the different BiMo oxide catalyst samples depending on the reactor used. As the fresh catalyst is exposed to the reaction gases, the depletion of the surface oxygen alters the structure of the BiMo oxide to reduce the amount of the α-phase present. As this change occurs, the activity and selectivity of the catalyst is reduced. The complete lack of the more active α-phase in the post-reaction FBR catalyst, combined with the presence of the α-phase in the post-reaction IMR catalyst, suggests that the selectivity in the IMR will be higher than the FBR because of the phases present.

In summary, the characterization results show clearly that the V/MgO and BiMo oxide catalysts change after exposure to reaction conditions. The XRD and XPS results correlate well with each other and demonstrate the reduced state of the catalyst following reaction. The changes to the V/MgO catalyst are only seen between the calcined catalyst and the two post-reaction catalyst samples. However, the BiMo oxide catalyst shows a large difference in the phases present between the calcined and post-reaction conditions between the FBR and IMR. The ability of the IMR design to maintain the presence of the active BiMo oxide phase under reaction conditions clearly demonstrates the potential benefits in improved selectivity for the IMR over the FBR.

5. Catalytic activity

5.1. Single-bed fixed bed reactor experiments

Single-bed catalytic fixed bed reactor experiments provide a basis of comparison to verify any effect due to the use of the membrane reactor. Time on stream experiments in fixed beds indicated that two hours time on stream were required to reach steady state activity. Our prior simulations [1] showed the O_2:HC ratio and

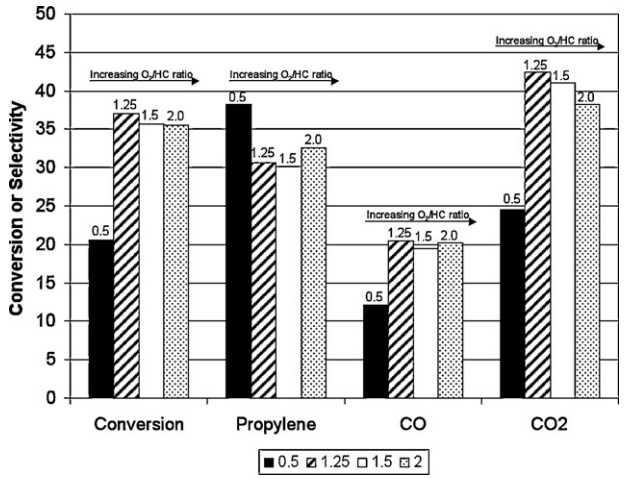

Fig. 5. Conversion and product selectivity for various O_2/HC ratios for the ODH of propane over the V/MgO catalyst in the FBR at 500 °C.

temperature to be the critical parameters in the selective oxidation reaction and these effects are the focus of these experiments. Gas phase reactions in the absence of a catalyst for both propane and propylene oxidation were found to be minimal and have been ignored for these studies.

5.2. Fixed bed oxidative dehydrogenation of propane

Conversion of propane and selectivity towards propylene, CO, and CO_2 are presented in Fig. 5 as the O_2:HC ratio vary from 0.5:1 up to 2:1. At the stoichiometric ratio, the conversion is 20% with selectivity to propylene of 38%. Increasing the ratio to 1.25 raises the conversion to about 35% but selectivity decreases to about 30%. Further increase of the O_2:HC ratio has no effect on conversion and selectivity as they remain at about 35% and 30%, respectively, up from an O_2:HC ratio of 2.

The ODH reaction selectivity is highest at the stoichiometric O_2:HC ratio of 0.5:1 which is consistent with the prior simulation results in our laboratory [1] and the reaction mechanisms proposed in literature [25,28,29].

Temperature effects on the conversion and selectivity of the ODH reaction are shown in Fig. 6. The conversion increases slightly from 15% at 450 °C to 20% at 500 °C whereas the selectivity to

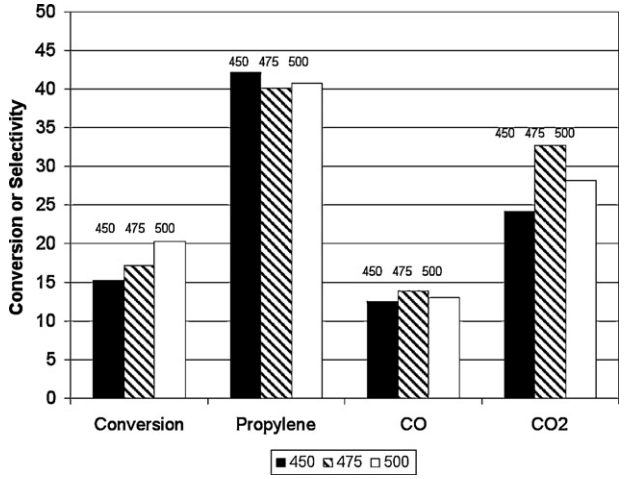

Fig. 6. Propane conversion and products selectivity for the ODH of propane reaction over the V/MgO catalyst in the FBR at 450 °C, 475 °C and 500 °C at an O_2:HC ratio of 1:2.

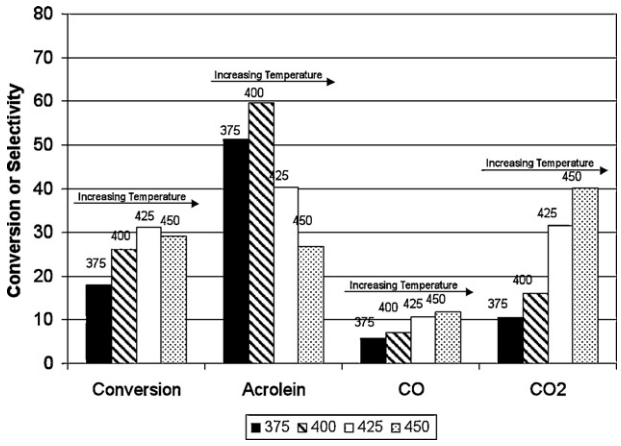

Fig. 7. Propene conversion and selectivity at various temperatures for POA reaction over the BiMo oxide catalyst in the FBR at an O_2:HC ratio of 1:1.

propylene is relatively constant with temperature, around 40%. The increase of the propylene yield (conversion × selectivity) is favorable and compensate any loss in selectivity, therefore subsequent studies were conducted under these optimal conditions (500 °C with an O_2:HC ratio of 0.5:1) for the ODH of propane over a V/MgO catalyst.

5.3. Fixed bed partial oxidation of propylene (POA) to acrolein

As with the ODH of propane, gas phase reactions were ignored due to less than 1% conversion of propylene in absence of a catalyst. Time on stream results of the POA reaction over the BiMo oxide catalyst showed that deactivation occurred over the first three hours time on stream before attaining a steady activity. For this reason, all data for the POA reaction are reported after three hours of time on stream. The XRD and XPS results previously discussed show a reduction in the ratio of the α-/γ-phases. Clearly the change in this ratio during the three hrs TOS prior to the steady state was responsible for change in activity and selectivity.

During the POA reaction, formation of CO_x is kinetically and thermodynamically favored, thus the O_2:HC ratio is again of importance. Experimentally it was found (not shown) that the optimum ratio equals the stoichiometric ratio of 1:1. The effect of temperature at the stoichiometric ratio, shown in Fig. 7, indicates that at temperatures above 400 °C, the selectivity of the BiMo oxide catalyst to acrolein is greatly reduced, from a maximum of 60% selectivity at 400 °C down to 27% at 450 °C. CO_x selectivity is proportional to the temperature as the CO_x selectivity continuously increases with increasing temperature. Propylene conversion reaches a maximum of 30% at 425 °C which corresponds to the temperature for complete oxygen conversion. The lack of an Arrhenius behavior is due to the deactivation behavior of the catalysts which as shown by the characterization behavior involves a phase change. These results indicate the POA reaction should be run between 400 °C and 425 °C at the stoichiometric ratio of 1:1 for oxygen and propylene as supported by prior simulations [1] and the proposed mechanisms in literature [30–33].

5.4. Single-bed inert membrane reactor experiments

5.4.1. IMR conversion during oxidative dehydrogenation of propane

The membrane reactors follow the trends seen in the FBR with respect to the O_2:HC ratio and temperature. One difference, shown in Fig. 8 for the ODH of propane, is that with increasing O_2:HC ratio, there is a gradual increase in conversion in the IMR along with a

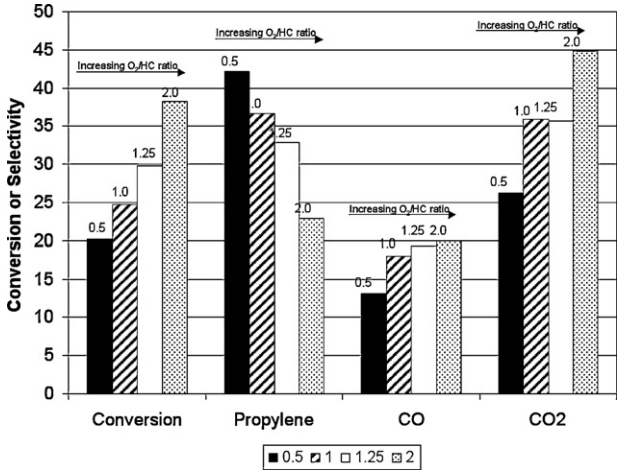

Fig. 8. Effect the O_2:HC ratio on propane conversion and oxidation product selectivity for the ODH of propane over the V/MgO catalyst in the IMR at 500 °C.

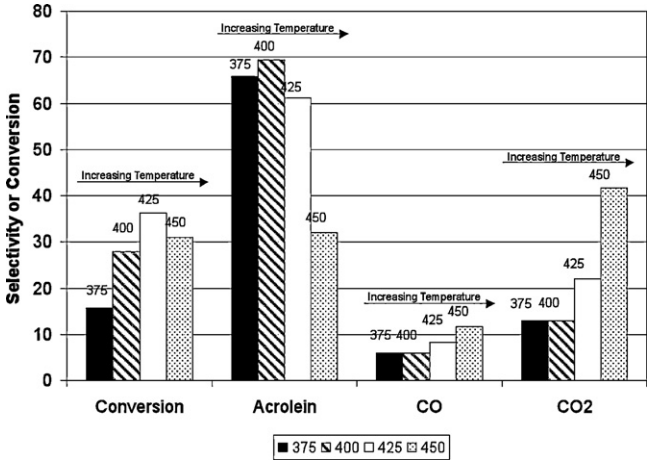

Fig. 10. Propylene conversion and product selectivity at various temperatures for the POA reaction to acrolein over BiMo in the IMR at an O_2:HC ratio of 1:1.

corresponding gradual decrease in the propylene selectivity. In the FBR, we observed a sharper increase in conversion and decrease in selectivity to propylene that reached a plateaux and remained constant as the oxygen ratio was increased. In the IMR, at a stoichiometric O_2:HC ratio of 0.5:1 a 20% conversion of propane and 42% selectivity to propylene was attained. Increasing the O_2:HC ratio increases the conversion up to 38%, but it reduces propylene selectivity to 23% with the corresponding increase in CO_x production.

Temperature effects in the IMR are similar to the trends observed in the FBRs and thus are not shown. Increasing temperatures in the membrane reactor increase conversion of propane and decrease the selectivity to propylene. As with the single-bed FBR results, the best yield for the ODH reaction are obtained at 500 °C with an O_2:HC ratio of 0.5:1. Comparison of the FBR and IMR under identical conditions for the ODH reaction shows the selectivity to propylene is slightly higher in the IMR than in the FBR.

5.4.2. IMR for the partial oxidation of propylene to acrolein

Adjusting the O_2:HC ratio for the POA reaction in the IMR reveals a maximum selectivity to acrolein at the stoichiometric value of 1:1, as shown in Fig. 9. The stoichiometric O_2:HC ratio produces a selectivity to acrolein of 69% while maintaining a low selectivity to CO_x (<20%). Increasing the oxygen above the stoichiometric value promotes the complete oxidation reactions and does not enhance the selective oxidation reaction to acrolein.

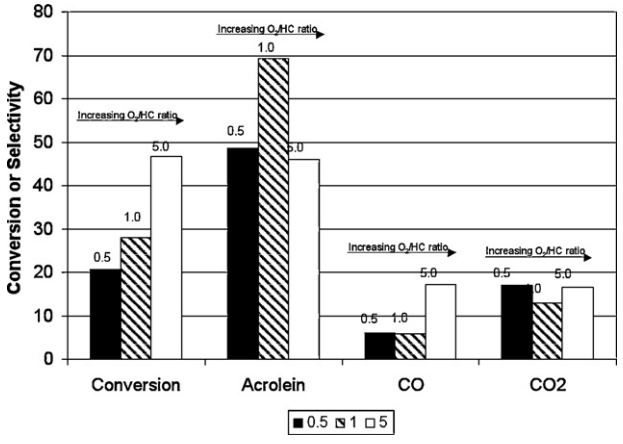

Fig. 9. Effect of the O_2:HC ratio during the propylene conversion and oxidation product selectivity for the POA to acrolein reaction over BiMo in the IMR at 400 °C.

The IMR exhibits the highest yield of acrolein between 400 °C and 425 °C (Fig. 10) while limiting the formation of CO_x. The single-bed experiments for the POA reaction in both the FBR and IMR attain the best results with a stoichiometric ratio of 1:1 and at temperatures between 400 °C and 425 °C. Comparing the selectivity to acrolein of the two reactor configurations, show that acrolein selectivity is higher by 10% in the IMR than in the FBR at both 400 °C and by 20% at 425 °C for the O_2:HC ratio of 1:1. The conversions are slightly different at 27% at 400 °C and 36% at 425 °C.

The single-bed experiments show the selectivity of the desired products in both the ODH and POA reactions are slightly higher in the IMR in comparison to the FBR. These improvements, while relatively small, suggest that the direct conversion of propane to acrolein reaction will result in larger improvements in selectivity in the dual bed membrane reactor.

5.4.3. Dual bed experiments for the propane to acrolein reaction

Dual bed experiments combine the catalyst bed for the ODH and POA reactions previously discussed in a single reactor. Dual bed FBR (2B-FBR) and dual bed IMR (2B-IMR) experiments were run under conditions similar to the optimum operating conditions determined through single-bed experiments. Therefore, the first bed for the ODH reaction was run at 500 °C with an initial O_2:HC ratio of 0.5:1 and a total flow rate of 100 cm^3/min, and the second bed for the POA reaction was run at 425 °C. In the 2B-FBR, the flow rate and O_2:HC ratio in the second (POA) catalyst bed are predetermined from the effluent from the ODH catalyst bed. However, in the 2B-IMR, oxygen was added to the POA catalyst bed through a membrane tube in the second bed to provide an O_2:HC ratio of 1:1 in the POA catalyst bed.

Dual bed reactors configurations were investigated first to determine the effect of adding a membrane bed first to the POA catalyst bed and then to both the ODH and POA catalyst beds. The best results were obtained with dual bed configurations with the a 2B-FBR resulted in a 3.5% acrolein selectivity and selectivity to propylene of ~19.5%, and a 2B-IMR yielded acrolein selectivity of 6.8% and propylene selectivity increased to 28.7%. Propane conversion decreased from 35% for the 2B-FBR, to 26% for the 2B-IMR.

While improvements in the acrolein selectivity were expected between the 2B-FBR and 2B-IMR based upon the single-bed experiment results, we also observed an increase in propylene selectivity. This can be explained as an additional conversion of the unconverted propane from the ODH bed on the POA bed.

Although the 2B-IMR is advantageous compared to the 2B-FBR, the selectivity to acrolein and the resulting yield are still low.

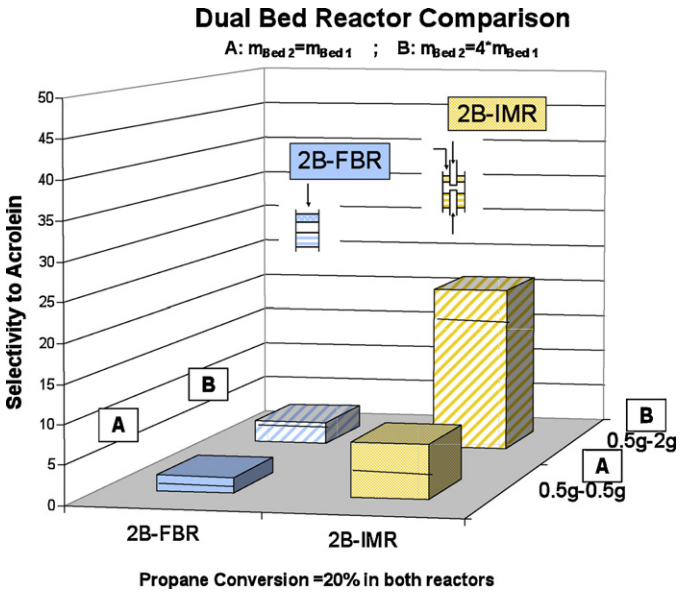

Fig. 11. Acrolein selectivity in the 2B-FBR and 2B-IMR. BiMo catalyst mass: (A) 0.5 g and (B) 2.0 g. Stoichiometric O_2:HC ratio and reactor bed temperatures of 500 °C and 425 °C, respectively.

The significantly high propylene selectivity however in the 2B-IMR indicates that there is potential for additional conversion of propylene to acrolein in the second bed. Increasing the mass of the POA catalyst bed is the easiest method to increase the conversion of propylene and thereby increasing acrolein selectivity. The initial dual bed reactor runs were performed with two equal catalyst beds of roughly 0.5 g. To promote the conversion of propylene in the POA catalyst bed, the BiMo catalyst mass was quadrupled to 2.0 g of catalyst Fig. 11. This increase of the catalyst mass had little improvement on the selectivity to acrolein in the 2B-FBR as it increased from 2% to 3% with the quadrupled BiMo catalyst bed. However, the increased bed mass had a significant effect on the 2B-IMR. The acrolein selectivity increased from a meager 6.9% to 21.5% at the same propane conversion. This increased acrolein selectivity was directly related to a simultaneous decrease in the propylene selectivity.

The larger catalyst mass also revealed a deactivation in the 2B-FBR that was not observed in the 2B-IMR under any conditions. The dashed outline in Fig. 11 represents the initial selectivity to acrolein in the 2B-FBR at the two different catalyst masses for the second reaction bed. With the 0.5 g catalyst bed in the 2B-FBR, the selectivity decreased from an initial value of 4.2% down to 2% during three hours of time on stream. However, the selectivity to acrolein in the quadrupled catalyst bed dropped from 15.3% to 2.9% after four hours time on stream. No such decrease in selectivity is observed in the 2B-IMR with the quadruple mass of BiMO catalyst.

It is proposed that this deactivation is due to the near complete conversion of oxygen in the 2B-FBR and little oxygen being subsequently available to reoxidize the active sites in the BiMo oxide catalyst during reaction conditions. The addition of a supplemental oxygen stream to the POA catalyst bed in the 2B-IMR reduces this deactivation and enables the 2B-IMR to maintain its initial activity and selectivity to acrolein. It should be noted, however, that the selectivity of the 2B-IMR to acrolein is always higher than that of the initial 2B-FBR selectivity at any of the experimental conditions. This is further supported by the characterization results of the BiMo oxide catalyst by XRD and XPS. The post-reaction FBR catalysts showed a more reduced BiMo catalyst, and thereby less active, than either the calcined or post-reaction IMR catalysts. The ability of the 2B-IMR to maintain the more active phase of the BiMo oxide arrests the deactivation of the catalyst and resulted in a much higher acrolein selectivity after 3 hrs TOS. Further optimization of catalysts and residence times could lead to even further conversion of propane to acrolein.

6. Conclusions

Single-bed and dual bed reaction studies demonstrated improvement of a given catalysts' selectivity by changing the reaction configuration from a traditional fixed bed to a membrane reactor. The membrane reactor provides higher selectivity and yield of the desired product than the fixed bed reactor in the ODH-POA and propane to acrolein in dual bed reactor systems. Distributing the oxygen through the use of the IMR was effective in reducing the local O_2:HC ratio in the reactor and subsequently increased the selectivity to the desired product. The versatile nature of the dual bed reactor system enabled the optimization of the yield to acrolein by varying the mass of catalyst and oxygen flow in the second bed. More interestingly, control of the oxygen in the second bed also prevents the deactivation of the POA catalyst in the dual bed reactor system. Due to its versatile nature and its catalyst independent effect, the membrane reactor holds the potential to be a useful tool in promoting the formation of the desired product in other catalytic selective oxidation reaction networks.

Acknowledgements

We gratefully acknowledge the support from the NSF grant CTS0224435 for funding this work.

References

[1] C.M. O'Neill, E.E. Wolf, Yield improvements in membrane reactors for partial oxidation reactions, Ind. Eng. Chem. Res. 45 (8) (2006) 2697–2706.
[2] G. Capannelli, E. Carosini, F. Cavani, et al., Comparison of the catalytic performance of V_2O_5, Chem. Eng. Sci. 51 (10) (1996) 1817–1826.
[3] X.T. Gao, P. Ruiz, Q. Xin, et al., Preparation and characterization of 3 pure magnesium vanadate phases as catalysts for selective oxidation of propane to propene, Catal. Lett. 23 (3–4) (1994) 321–337.
[4] R.X. Valenzuela, V.C. Corberan, On the intrinsic activity of vanadium centres in the oxidative dehydrogenation of propane over V–Ca–O and V–Mg–O catalysts, Top. Catal. 11 (1–4) (2000) 153–160.
[5] W. Schuster, J.P.M. Niederer, W.F. Hoelderich, The gas phase oxidative dehydrogenation of propane over TS-1, Appl. Catal. A: Gen. 209 (1–2) (2001) 131–143.
[6] M.A. Chaar, D. Patel, M.C. Kung, et al., Selective oxidative dehydrogenation of butane over V–MgO catalysts, J. Catal. 105 (2) (1987) 483–498.
[7] D.S.H. Sam, V. Soenen, J.C. Volta, Oxidative dehydrogenation of propane over V–MgO catalysts, J. Catal. 123 (2) (1990) 417–435.
[8] A. Corma, J.M.L. Nieto, N. Paredes, Influence of the preparation methods of V–MgO catalysts on their catalytic properties for the oxidative dehydrogenation of propane, J. Catal. 144 (2) (1993) 425–438.
[9] H.W. Zanthoff, M. Lahmer, M. Baerns, et al., Enhanced product selectivity in partial oxidation of propane on multicomponent oxide catalysts by masking of total oxidation sites, J. Catal. 172 (1) (1997) 203–210.
[10] J.R. Monnier, G.W. Keulks, The catalytic-oxidation of propylene, the kinetics and mechanism over beta-$Bi_2Mo_2O_9$, J. Catal. 68 (1) (1981) 51–66.
[11] Z. Magagula, E. van Steen, Time on stream behavior in the (amm)oxidation of propene, Catal. Today 49 (1–3) (1999) 155–160.
[12] M. Allen, R. Betteley, M. Bowker, et al., The partial oxidation of propene on Fe, Catal. Today 9 (1–2) (1991) 97–104.
[13] C. Daniel, G.W. Keulks, Catalytic-oxidation of propylene. 2. Iron-based bismuth molybdate catalysts for partial oxidation of propylene, J. Catal. 29 (3) (1973) 475–478.
[14] E. van Steen, M. Schnobel, R. Walsh, et al., Time on stream behavior in the partial oxidation of propene over iron antimony oxide, Appl. Catal. A-Gen. 165 (1–2) (1997) 349–356.
[15] P. Kolsch, M. Noack, R. Schafer, et al., Development of a membrane reactor for the partial oxidation of hydrocarbons: direct oxidation of propane to acrolein, J. Membr. Sci. 198 (1) (2002) 119–128;
Q. Kölsch, M. Smejkal, R. Noack, J. Schäfer, Caro: partial oxidation of propane to acrolein in a membrane reactor—experimental data and computer simulation, Catal. Commun. 3 (2002) 465–470.
[16] A. Kaddouri, C. Mazzocchia, E. Tempesti, The synthesis of acrolein and acrylic acid by direct propane oxidation with Ni–Mo–Te–P–O catalysts, Appl. Catal. A: Gen. 180 (1–2) (1999) 271–275.

[17] M. Baerns, O.V. Buyevskaya, M. Kubik, et al., Catalytic partial oxidation of propane to acrolein, Catal. Today 33 (1–3) (1997) 85–96.
[18] Y.C. Kim, W. Ueda, Y. Morooka, Catalytic (amm)oxidation of propane with molecular-oxygen over complex metal-oxides—involvement of homogeneous reaction in gas-phase, Catal. Today 13 (4) (1992) 673–678.
[19] M.Y. Sinev, O.V. Udalova, Y.P. Tulenin, et al., Propane partial oxidation to acrolein over combined catalysts, Catal. Lett. 69 (3–4) (2000) 203–206.
[20] T. Shishido, T. Konishi, I. Matsuura, et al., Oxidation and ammoxidation of propane over Mo–V–Sb mixed oxide catalysts, Catal. Today 71 (1–2) (2001) 77–82.
[21] T.P. Snyder, C.G. Hill, The mechanism for the partial oxidation of propylene over bismuth molybdate catalysts, Catal. Rev.-Sci. Eng. 31 (1–2) (1989) 43–95.
[22] R.K. Grasselli, Selectivity and activity factors in bismuth-molybdate oxidation catalysts, Appl. Catal. 15 (1) (1985) 127–139.
[23] T.G. Alkhazov, K.Y. Adzhamov, L.Y. Margolis, et al., Comparison of the structure and catalytic activity of different samples of the Bi–Mo oxide system, Kinet. Catal. 18 (3) (1977) 496.
[24] J.F. Moulder, Handbook of X-ray Photoelectron Spectroscopy, Perkin Elmer Corp., 1992.
[25] R. Grabowski, J. Sloczynski, Kinetics of oxidative dehydrogenation of propane and ethane on VO_x, Chem. Eng. Process. 44 (10) (2005) 1082–1093.
[26] K. Routray, K.R.S.K. Reddy, G. Deo, Oxidative dehydrogenation of propane on V_2O_5/Al_2O_3 and V_2O_5, Appl. Catal. A: Gen. 265 (1) (2004) 103–113.
[27] R.P. Singh, M.A. Banares, G. Deo, Effect of phosphorous modifier on V_2O_5, J. Catal. 233 (2) (2005) 388–398.
[28] E.K. Novakova, J.C. Vedrine, E.G. Derouane, Propane oxidation on Mo–V–Sb–Nb mixed-oxide catalysts. 1. Kinetic and mechanistic studies, J. Catal. 211 (1) (2002) 226–234.
[29] D.L. Stern, R.K. Grasselli, Reaction network and kinetics of propane oxydehydrogenation over nickel cobalt molybdate, J. Catal. 167 (2) (1997) 560–569.
[30] G.W. Keulks, M.Y. Lo, Catalytic-oxidation of propylene. An investigation of the kinetics and mechanism over iron antimony oxide, J. Phys. Chem. 90 (20) (1986) 4768–4775.
[31] G.W. Keulks, M.P. Rosynek, C. Daniel, Bismuth molybdate catalysts–kinetics and mechanism of propylene oxidation, Ind. Eng. Chem. Prod. Res. Dev. 10 (2) (1971) 138–142.
[32] G.W. Keulks, J.L. Hall, C. Daniel, et al., Catalytic-oxidation of propylene. 4. Preparation and characterization of alpha-bismuth molybdate, J. Catal. 34 (1) (1974) 79–97.
[33] J.L. Callahan, R.K. Grassell, E.C. Milberge, et al., Oxidation and ammoxidation of propylene over bismuth molybdate catalyst, Ind. Eng. Chem. Prod. Res. Dev. 9 (2) (1970) 134–142.